STRESS OPTIMIZATION OF COUPLING PINS FOR LARGE DIAMETER REAMING TOOL OF COAL-BED METHANE WELL

Shu-Lin Liu[1], Rui Liu[1], Xue-Hong Zhang[2], JI-Cheng Liu[1], Hai-Tao Jiang[3], Jun-Ran Zhou[3]
[1] *School of Mechatronics Engineering and Automation, Shanghai University, Shanghai, P. R. China*
[2] *Shanghai Volkswagen Co. Ltd, Shanghai, P. R. China*
[3] *Bohai Drilling and Exploration Company, Tianjin, P. R. China*
E-mail: lsl346@shu.edu.cn; zhangxuehong_2004@163.com

Received May 2010, Accepted October 2011
No. 10-CSME-31, E.I.C. Accession 3194

ABSTRACT

The paper focuses on the dynamics optimization of the pin joints which determine the operating performance and life of a novel Large-diameter Coal-bed Methane Reaming Tool (LCMRT). For this purpose, the constraint force equations of the pin joints for LCMRT are first established using Newton-Euler dynamics theory. Moreover, the virtual prototype model of LCMRT is created for dynamics simulations. Based on the dynamics simulations, the constraint forces of the pin joints are shown. Size optimization results for LCMRT are exhibited and described in detail through parametric model. Finally, the results of dynamics simulations based on the LCMRT optimized are demonstrated to validate optimization effect.

Keywords: dynamics optimization; LCMRT; dynamics simulation.

OPTIMISATION DU STRESS DES GOUPILLES D′ACCOUPLEMENT D′UN OUTIL D′ALÉSAGE DE GRAND DIAMÈTRE DANS LES PUITS DE GAZ DE MÉTHANE

RÉSUMÉ

L′article porte sur l′optimisation dynamique des goupilles d′accouplement qui déterminent la performance et la durée de vie d′un outil d′alésage de grand diamètre dans les puits de gaz de méthane. À cette fin, on établit les forces de contrainte des goupilles d′accouplement en se servant de la théorie de la dynamique de Newton-Euler. De plus, un modèle prototype virtuel est élaboré pour les simulations dynamiques. En se basant sur ces simulations dynamiques, nous démontrons les forces de contrainte des goupilles d′accouplement. Les résultats sont établis et expliqués en détail pour un modèle paramétrique; et finalement, les résultats des simulations dynamiques sont présentés pour valider l′effet de l′optimisation.

Mots-clés : optimisation dynamique; LCMRT; simulation dynamique.

INTRODUCTION

With the exhaustion of resources such as oil and natural gas, the exploitation of coal-bed methane (CBM) becomes increasingly urgent [1]. So far, lots of countries have made great efforts on the mining technology of coal-bed methane [2]. During coal-bed methane exploitation, the larger hole diameter, the more production. Therefore, it is necessary to adapt open-hole cavity completion and large diameter reaming tool [3].

In the last few years, the study of reaming tools has achieved great development [4]. According to the different ways of caving hole, reaming tools can be divided into reaming-while- drilling tool and barefoot reaming tool [5].

The research of reaming tools can be traced back to the early 1990s. Kalloo et al. [6] presented a novel bi-center bit reamer which have drilled deep exploration wells off the East Coast of Trinidad successfully. Sketchler et al. [7] introduced New Bi-Center Technology which proved validity in slim horizontal wells. Warren et al. [8] reviewed the Simultaneous Drilling and Reaming with Fixed Blade Reamers. Billman et al. [9] summarized a eccentric tool which increased liner size capacity in challenging salt dome application allowing longest horizontal well in Gulf of Suez. Halliburton Company invented the Under Reamer (URTM) tool which was a heavy-duty tool for enlarging borehole significantly beyond bit diameter. The URTM tool offers a variety of options for well completion design because it can be selectively activated or deactivated. The URTM tool can enhance production by expanding the hole for gravel packing, scraping filter cake, plus enabling gas storage underground.

The reaming-while-drilling tool has many advantages. For example, pilot hole is not necessary while enlarging a hole to reduce the cost of project. Moreover, there are not movable parts in the reaming-while-drilling tool to eliminate the falling risk of items. Therefore the cost of fishing up is reduced and loss of working time is avoided during construction. Meanwhile, some disadvantages of the reaming-while-drilling tool still exist. First, the penetration rate of reaming-while-drilling tool is lower compared with that of conventional drilling, which will definitely affect the overall drilling efficiency. Secondly, the tool wears excessively because of irrational mechanical structure. Thirdly, the tool could not control well path effectively due to structural and operational limits. Above all, the reaming-while-drilling tool cannot meet the demand of large-diameter cavity.

In recent years, barefoot reaming tools have been improved greatly to meet the increasing demand. At the end of 1990s, Jiaozuo Coal Mining Administration and Coal Research Institute in China designed the BZ-150 Automatic Reducing reaming drill bit successfully, which significantly improved the effect of relieving the coal seam gas pressure and gas drainage via increasing hole diameter. In 2004, Shengli Drilling Technology Research Institute successfully invented a hydraulic-mechanical barefoot reaming tool YKCD152-500, whose maximum enlarged hole diameter is 650 mm [10]. Although the coal-bed methane reaming tool significantly promotes the progress of well completion and increases the production of coal-bed methane, there are some problems when making a large-diameter hole. The capacity of existing drilling machine is not sufficient enough to ensure drilling depth and the drilling rod is easy to break down because of weak anti-torques of drill pipe and the arbor pin. In addition, its diameter is limited in 800 mm or so and it is difficult to get further development. Therefore, the new LCMRT was developed by Bohai Drilling Engineering and Technology Research Institute, through technology cooperation with Shanghai University. The LCMRT could make the hole in diameter of 2 m. Figure 1 shows the folded and unfolded states of LCMRT.

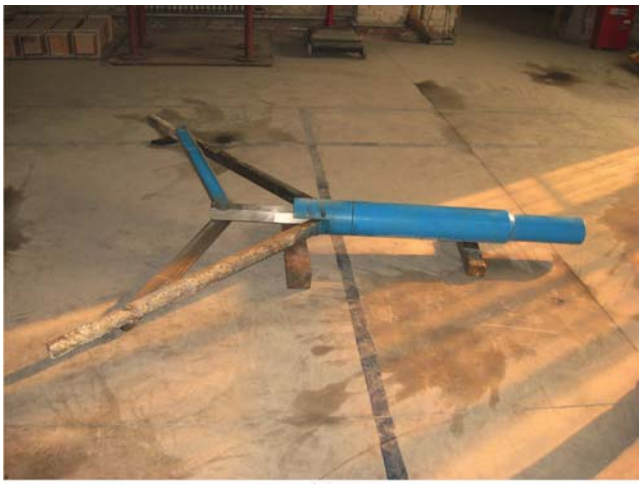

(a)

(b)

Fig. 1. Physical prototype of LCMRT: (a) Folded state of LCMRT, (b) Unfolded state of LCMRT.

The LCMRT has been applied in thickened oil F200VP of Xinjiang Kelamayi oilfield and made a hole in diameter of 2 m. Preliminary tests show that the pins are the weak link of LCMRT and subject to damage. Due to the limits of space and structure, the pin diameters could not increase, so the structural parameter of LCMRT should be studied to decrease the stress of pins. Based on dynamics simulations results of pins in different work conditions, the pin joint constraint forces are investigated, the LCMRT parametric model is built and its mechanical structure is optimized in the paper.

1. STRUCTURAL FEATURES AND OPERATIONAL PRINCIPLES OF LCMRT

The LCMRT was designed to satisfy the requirement of caving variable diameter well in simple structure. The schematic structure of LCMRT is shown in Fig. 2(b). The reaming part of LCMRT is composed of cutter bars and connecting rods, rather than complex roller cones and holding device. As is known to all, the larger the well diameter is, the greater the stress to the tool. So the structure of LCMRT is devised on purpose, as shown in Fig. 2(b). The structure arrangement can make the tool cave holes in diameter 1000 mm–2000 mm. Connecting bar,

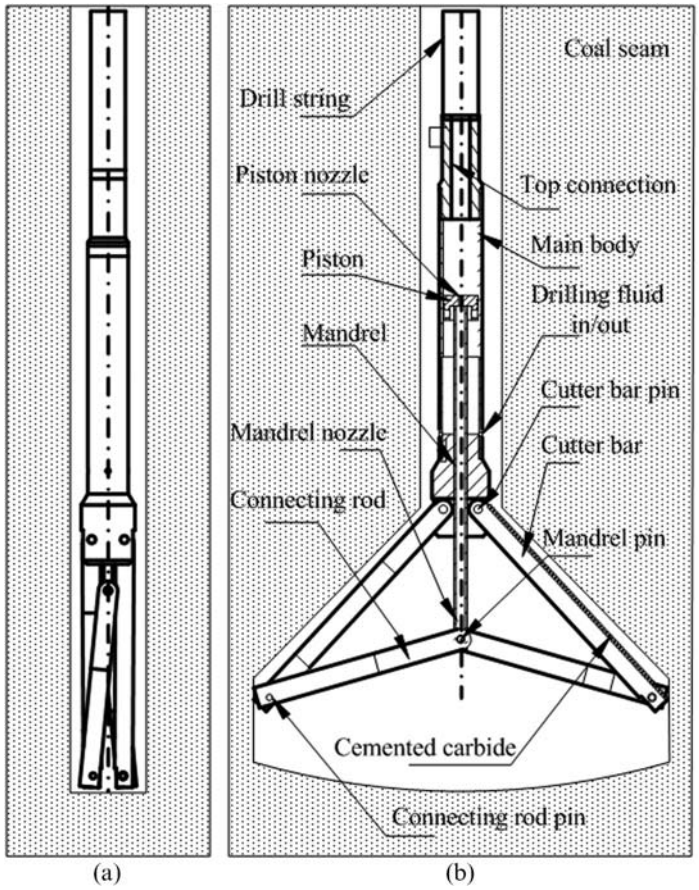

Fig. 2. Schematic structure of the LMRT: (a) initial state; (b) working state.

cutter bar, main body and mandrel are joined by coupling pins, so it is convenient to employ substitute parts.

Figure 2 illustrates the workflow of LCMRT. Figure 2(a) shows the initial condition. The top of LCMRT is attached to the drill unit which includes rotary system, circulating system and lifting system. When the LCMRT is delivered to operating position by drill system, the LCMRT will rotate, move vertically and extend its cutter bars under the control of drill system. The next phase in the workflow is the caving phase as shown in Fig. 2(b). The spinning LCMRT is lifted, the cutter bars are outspread and begin cutting the coal seam. The caving phase will continue till the diameter and depth meet the engineering requirements. Finally, the LCMRT constructs a larger cave, whose top surface is tapered and bottom is cambered. Meanwhile, the cutter bars of LCMRT will be unfolded by lowering the mud pressure.

2. DYNAMICS ANALYSIS OF LCMRT PIN JOINTS

2.1. Joint Constraint Force Analysis Considering Inertial Force

As is illustrated in Fig. 3, the LCMRT dynamic model is established by simplifying its complex structure as a double-slider crank mechanism. In Fig. 3, The coordinate system (x-A-y) is fixed in the space as shown in Fig. 3. m_1, m_2, m_3 and m_4 are the mass of cutter bar, connecting rod and mandrel and main body respectively. J_1 and J_2 are rotary inertia of cutter bar (AB) and connecting rod (BC) respectively. (x_1, y_1) and (x_2, y_2) describe the center-of-mass coordinates of

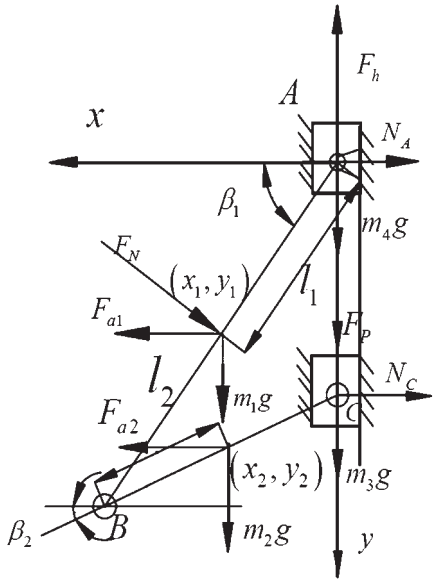

Fig. 3. Simplified dynamic model of LCMRT.

cutter bar and connecting rod respectively. l_1 and l_2 denote the length from center of cutter bar to point A and from center of connecting rod to point B respectively. β_1 and β_2 describe cutter bar included angle and connecting rod included angle to x-axis. The normal force acted on cutter bar is $F_{N,}$ the mud pushing force applied to piston is $F_{p,}$ and the lift force raising the LCMRT is $F_{h.}$. Furthermore, according to the force balance principle, F_h=0.5F_H is obtained.

Based on the dynamic model of LCMRT, the force exerted on every part will be analyzed, regardless of the friction of all the joints [12].

The free-body diagram for the cutter bar is shown in Fig. 4.

Applying the Newton′s second law for the cutter bar, the dynamic equilibrium equations is the following.

$$\begin{cases} F_{Ax} - F_{Bx} + F_{a1} + F_N \sin\beta_1 = 0 \\ F_{Ay} + m_1 g - F_{By} + F_N \cos\beta_1 = 0 \end{cases} \tag{1}$$

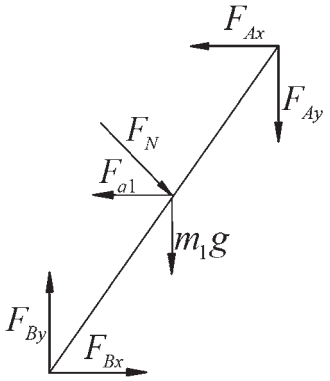

Fig. 4. Free-body diagram for the cutter bar.

Where, F_{a1} is centrifugal force of cutter bar. F_{Ax} and F_{Bx} are the components of constraint forces on point A and B along the x-axis respectively. F_{Ay} and F_{By} are the components of constraint forces on point A and B along the y-axis respectively.

The free-body diagram for the connecting rod is shown in Fig. 5.

Based on the force analysis of connecting rod, the dynamic equilibrium equations can be obtained as follows.

$$\begin{cases} F_{Bx} + F_{Cx} + F_{a2} = 0 \\ F_{By} + m_2 g + F_{Cy} = 0 \end{cases} \tag{2}$$

Where, F_{a2} is centrifugal force of connecting rod. F_{Cx} and F_{Cy} are the components of constraint force on point C along the x-axis and y-axis respectively.

The free-body diagram for the mandrel is shown in Fig. 6.

The dynamic equilibrium equations of mandrel can be written as

$$\begin{cases} F_P + m_3 g - F_{Cy} = 0 \\ N_C = -F_{Cx} \end{cases} \tag{3}$$

Where N_c is the force that the main body acts on the mandrel.

From Eqs. (1–3) above, the joint constraint force dynamics relationships with the included angles can be calculated.

2.2. Joint Constraint Force Analysis Considering Joint Clearances

Even with the most precise design, when the LCMRT is converted into prototype, there will be inevitable joint clearances caused by manufacturing tolerance and deflection of components, all of which affect the mechanical property of LCMRT.

The clearance may cause discontinuous contact of pin and pinhole, namely the relative penetration or free-flight mode. In order to analyze the contact force, it′s supposed that pin and pinhole are in continuous contact mode, because the time of discontinuous contact is very short. In the continuous contact mode, the clearance r is always constant, but the contact point is different.

The force diagram of LCMRT considering joint clearances is shown in Fig. 7. The normal force functioned on cutter bar is F_N, the mud pushing force applied to piston is F_p and the lift force of LCMRT is F_h. r_A, r_B and r_C define the radius clearance of cutter bar pin, mandrel pin and connecting rod pin respectively. The constants l_{AB} and l_{BC} are the lengths of cutter bar (AB) and connecting rod (BC), respectively. S_1 and S_2 is the mass center of cutter bar and connecting

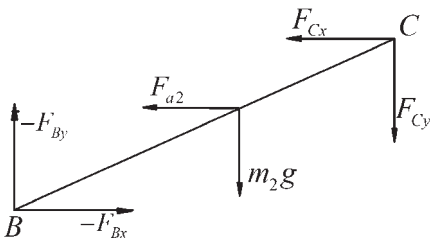

Fig. 5. Free-body diagram for the connecting rod.

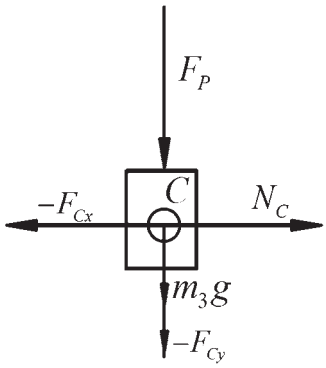

Fig. 6. Free-body diagram for the mandrel.

rod respectively. β_1 and β_2 describe cutter bar included angle and connecting rod included angle to x-axis respectively.

From the force diagram considering joint clearances, the force balance equation of cutter bar can be written as

$$\begin{cases} F_{Ax1} - F_{Bx1} - F_N \sin\beta_1 = 0 \\ F_{Ay1} + m_1 g - F_{By1} + F_N \cos\beta_1 = 0 \end{cases} \tag{4}$$

The force balance equation of cutter bar can be written as

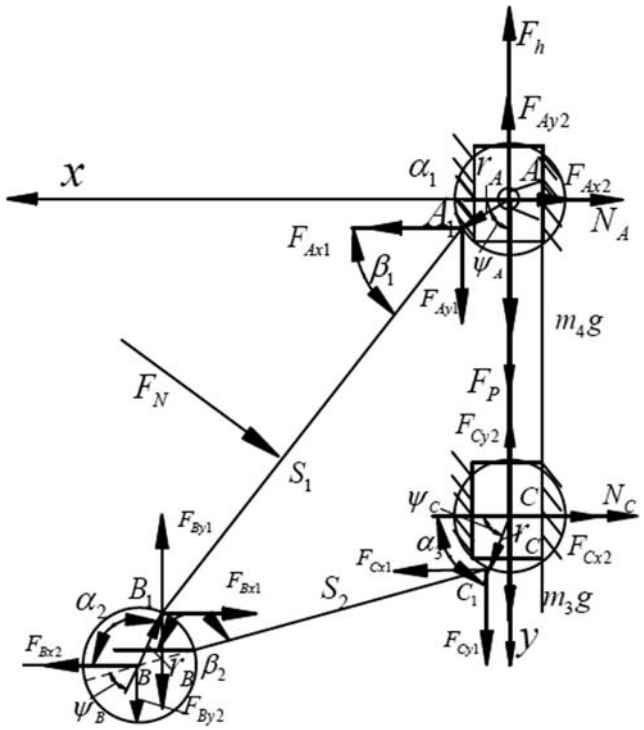

Fig. 7. Free-body diagram of LCMRT considering joint clearances.

$$\begin{cases} F_{Cx1} - F_{Bx2} = 0 \\ F_{By2} + m_2 g + F_{Cy1} = 0 \end{cases} \tag{5}$$

The force balance equation of mandrel can be written as

$$\begin{cases} F_{Cx2} + N_{C1} = 0 \\ F_P + m_3 g - F_{Cy2} = 0 \end{cases} \tag{6}$$

The force balance equation of main body can be written as

$$\begin{cases} -F_H + m_4 g - F_{Ay2} = 0 \\ F_{Ax2} + N_A = 0 \end{cases} \tag{7}$$

Where, m_1, m_2, m_3 and m_4 are the mass of cutter bar, connecting rod, mandrel and main body respectively. F_{Ax1}, F_{Ay1}, F_{Bx1} and F_{By1} are the axial components of forces acted on cutter bar at point A and B respectively. F_{Bx2}, F_{By2}, F_{Cx1} and F_{Cy1} are the axial components of forces acted on connecting rod at point B and C respectively. N_A is the force that coal seam acts on main body and N_{C1} is the force that main body acts on the mandrel.

According to the linearization theory, the equation of the normal force P^n and tangential force P^t generated by the contact can be obtained as

$$\begin{cases} F_x = -P^n \cos\psi - P^t \sin\psi \\ F_y = -P^n \sin\psi - P^t \cos\psi \end{cases} \tag{8}$$

Where F_x and F_y are the axial components of F, ψ is the angle contained by P^n and x-axis. Based on the equations above, the force equation of cutter bar pin considering clearance is

$$\begin{cases} F_{Ax1} - F_{Ax2} = -P^n_{41} \cos\psi_A - P^t_{41} \sin\psi_A \\ F_{Ay1} - F_{Ay2} = -P^n_{41} \sin\psi_A - P^t_{41} \cos\psi_A \end{cases} \tag{9}$$

The force equation of connecting pin considering clearance is

$$\begin{cases} F_{Bx1} - F_{Bx2} = -P^n_{21} \cos\psi_B - P^t_{21} \sin\psi_B \\ F_{By1} - F_{By2} = -P^n_{21} \sin\psi_B - P^t_{21} \cos\psi_B \end{cases} \tag{10}$$

The force equation of mandrel pin considering clearance is

$$\begin{cases} F_{Cx1} - F_{Cx2} = -P^n_{23} \cos\psi_C - P^t_{23} \sin\psi_C \\ F_{Cy1} - F_{Cy2} = -P^n_{23} \sin\psi_C - P^t_{23} \cos\psi_C \end{cases} \tag{11}$$

3. DYNAMICS MODELING AND SIMULATION

3.1. Virtual Prototype Modeling of LCMRT

According to the size of LCMRT, three dimensional model of each part was established and assembled. The model of LCMRT was imported into the ADAMS/View software through interface module. The positions of the mass, mass center and moment of inertias can be calculated by ADAMS/View software. The joints among the parts, such as revolute pair, translational pair and cylindrical pair, are defined based on the simplified dynamic model in Fig. 2. As shown in Fig. 8 is the virtual prototype modeling of LCMRT.

Material of LCMRT is 45#steel, and elastic modulus E is 210 Gp_a, Poisson′s ratio μ and density ρ are 0.29 and 7.8×10^3 kg/m^3 respectively. Table 1 shows the mass parameters of the model.

3.2. Dynamic Simulation

When the cutter bars of LCMRT cut coal seam, it is difficult to simulate the real working condition due to complex factors. In this paper, the load is simplified as the normal pressure perpendicular to cutter bar and the cutting force tangent to the direction of rotation. F_1 or F_2 represents the normal force between cutter bar and coal seam, ranging from 5.0×10^3 N to 2.0×10^3 N. In addition, F_3 or F_4 expresses the cutting force which changes from 3.0×10^3 N to 4.5×10^3 N.

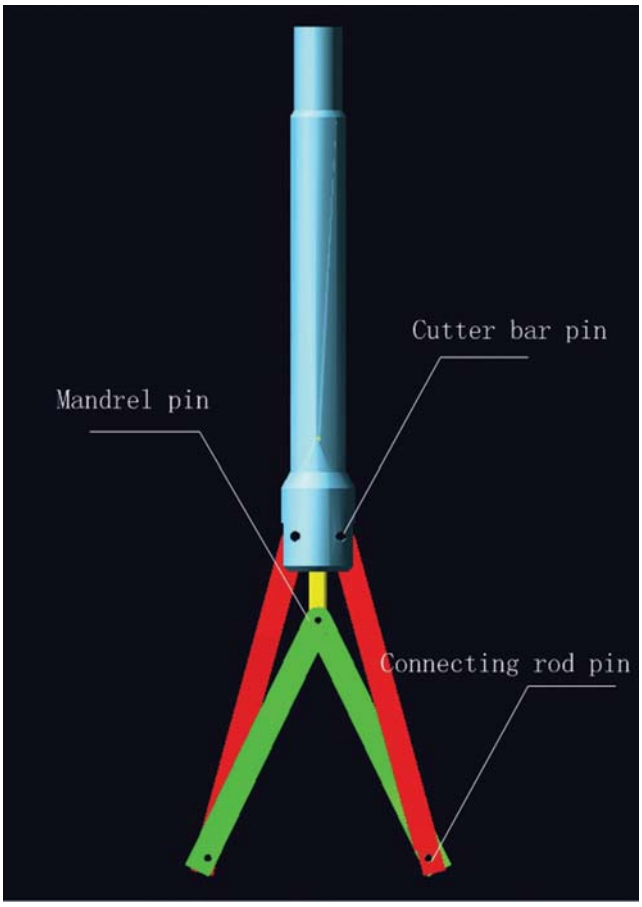

Fig. 8. Virtual prototype of LCMRT.

Table 1. Mass parameters of the model.

Part name	Main body	Cutter bar	Connecting rod	mandrel
mass(kg)	292.2	86.9	55.7	69.6

To analyze the forces under different condition, the values of forces at different joints are measured in different included angles ranging from 0° to 90° with 10° step interval. In the process of simulations, the normal forces and cutting forces should be applied on the cutting bars. The contact forces should be acted on all the pin joints, setting the contact stiffness as 2.0×10^{11} Pa, frictional factor as 0.1 and penetration depth as 0.001 m. Set the rotational speed of cylindrical joint as 360 °/s and simulation time as 1 s with 100 steps.

3.2.1. Dynamics Performance of LCMRT Unoptimized

When LCMRT is transferred to the bottom of well by drill strings, it will gradually rotate and then extend the cutter bars under drill system control. If the value of instrument board drops drastically, it represents that LCMRT has completed a segment. To obtain the stress laws of LCMRT, the simulation of whole completion process is carried out.

The stress laws of pin joints are shown in Figs. 9–11.

Figures 9–11 indicated that the overall stresses on the pin joints decrease with the included angle increasing, while the local stress value is fluctuating greatly. The stress reaches a relatively stable value when the include angle reaches the max. It should be noted that the impact of local stress is harmful to LCMRT′s life, so the optimization of LCMRT structure should be done to diminish the impact of local stress.

3.2.2. Analysis of Dynamics Simulation

According the early simulation analysis, the structure of this model is unreasonable, so it is necessary that the structure should be optimized through modifying the size and dimension of LCMRT.

Based on the data of simulation above, the relation between the joint constraint forces and other parameters can be obtained.

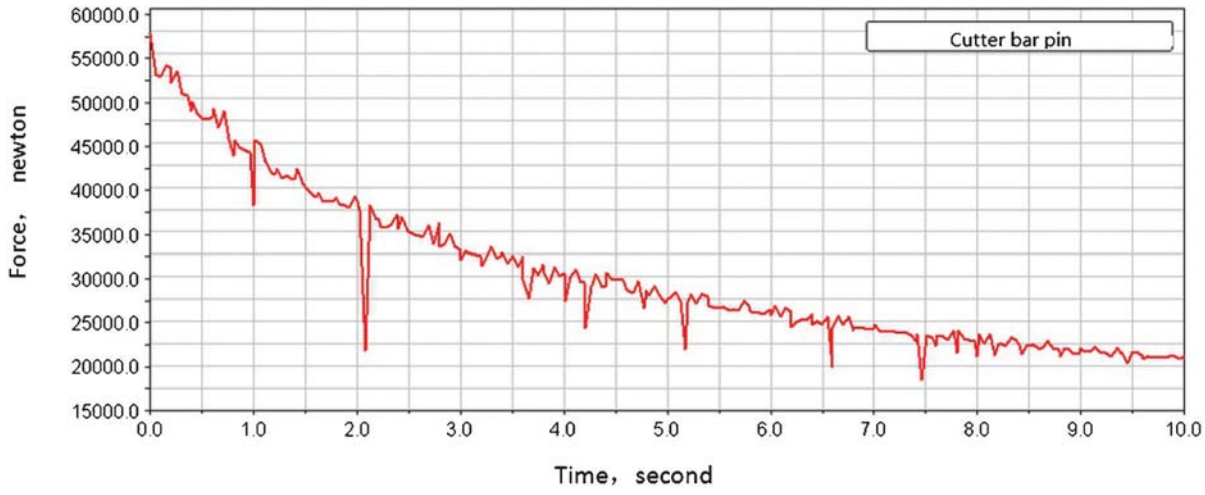

Fig. 9. Stress curve of cutter bar pin.

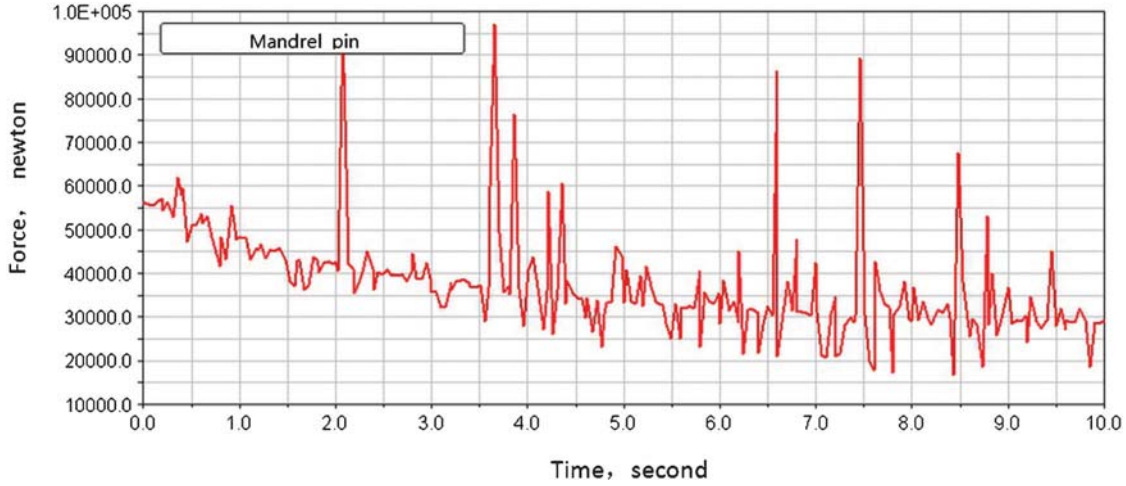

Fig. 10. Stress curve of mandrel pin.

(1) The relation between included angle and joint constraint force

When $F_1=F_2=27000$ N, $F_3=F_4=15000$ N, the dynamic simulations were carried out in different included angles ranging from 0° to 90°. The relation between included angle and joint constraint force can be obtained, as described in Fig. 12.

(2) The relation between normal force and joint constraint force

Set the included angle as 30°, and $F_3=F_4=\mu F_1=\mu F_2$. When the normal force F_1 grows from 5000 N to 20000 N, the relation between joints constraint forces and the normal force F_1 can be obtained from the simulation results, as shown in Fig. 13.

(3) The relation between cutting force and joint constraint force

When included angle is 30° and the normal force values range from 5000 N to 20000 N, the relation between cutting force and joint constraint force can be obtained from simulation, as shown in Fig. 14.

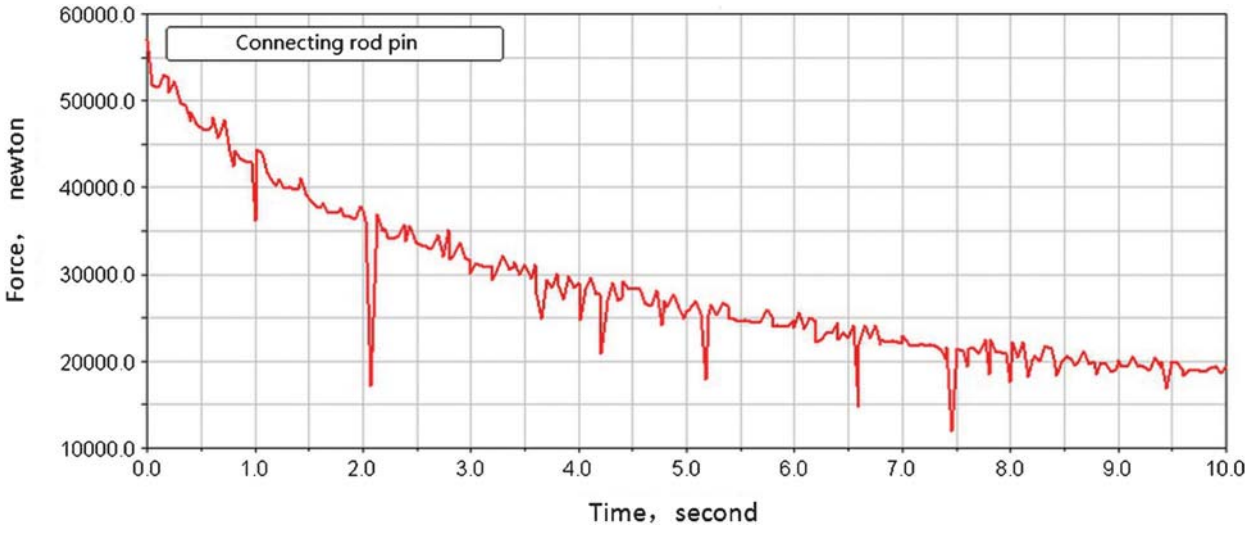

Fig. 11. Stress curve of connecting rod pin.

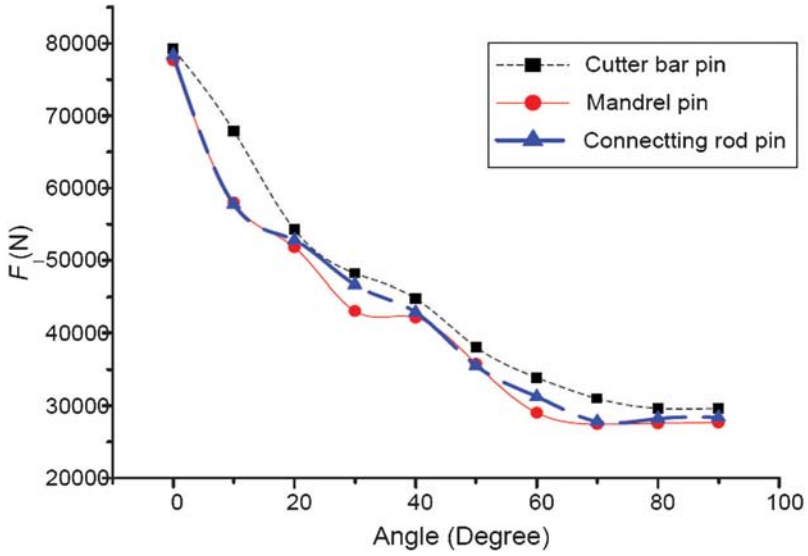

Fig. 12. Relation between included angle and joint constraint force.

Based on the Fig. 14, it can be concluded that the cutting forces have little effect on the joint constraint forces. It can be seen that the torque plays a weak role in the process of completion. On the other hand, the normal forces significantly affect the strength performance of joints. The results validate that the cutting force and frictional torque generated by coal seam is mainly passed on to main body. Therefore, the impact of normal pressure on joints should be studied well. The investigation includes the structure improvement and optimization to reduce the impact of normal pressure.

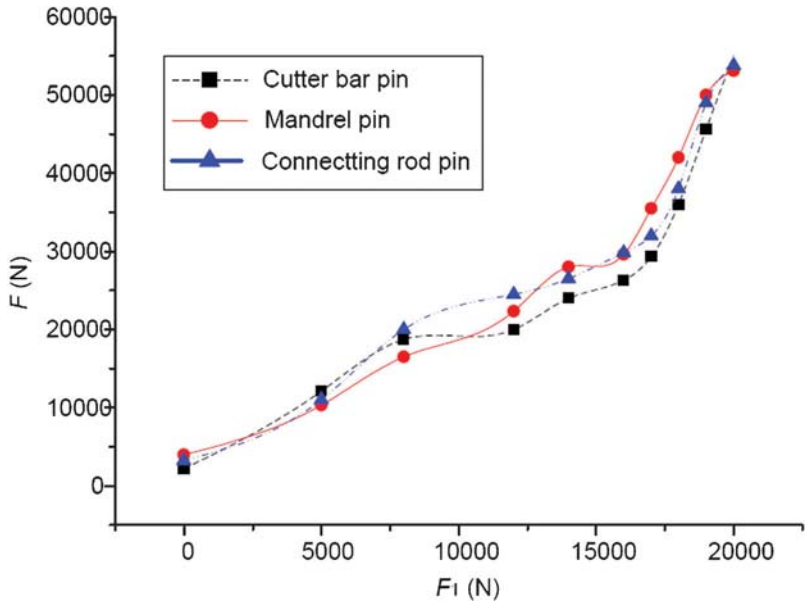

Fig. 13. Relation between normal force and joint constraint force with 30° included angle.

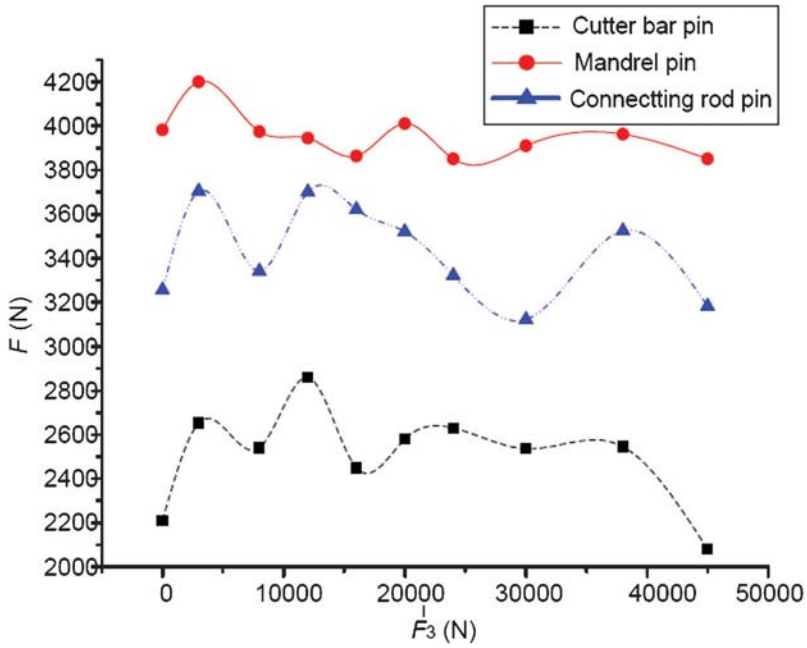

Fig. 14. Relation between cutting force and joint constraint force with 30° included angle.

4. DYNAMIC PERFORMANCE OPTIMIZATION OF LCMRT

4.1. Optimization Objective

In the process of caving well hole, the pins are subject to damage because of the gradually increasing force when the diameter of well hole becomes larger. To solve this problem, the mechanical structural should be optimized. The optimization objective is to lower the force acting on the pins to reduce the probability of the damage, in the case that the max caving diameter is 2000 mm.

From the analysis of dynamic simulation, it is known that the force acting on the pins mostly relates to the length of bars and included angle. To study the relationship in detail, the length of bar should be parameterized and the effect of the rod length on the joint force should be analyzed.

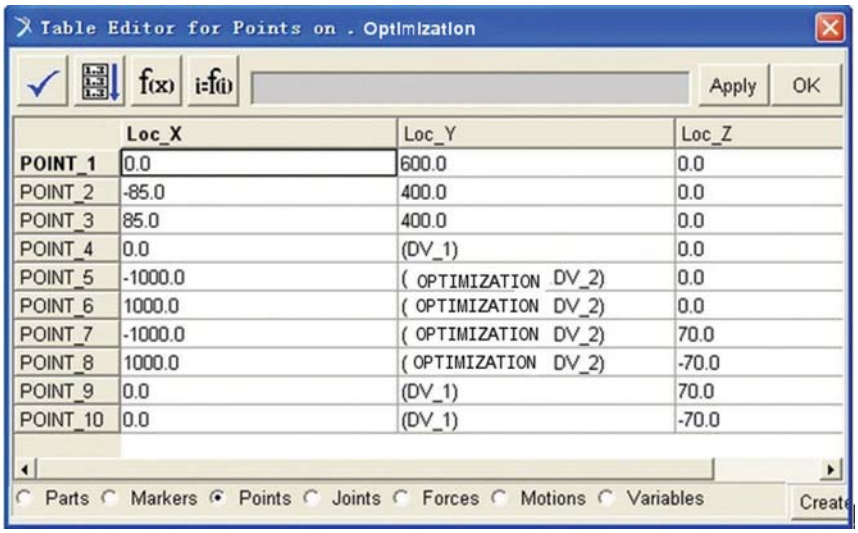

Fig. 15. Creation of optimization parameters.

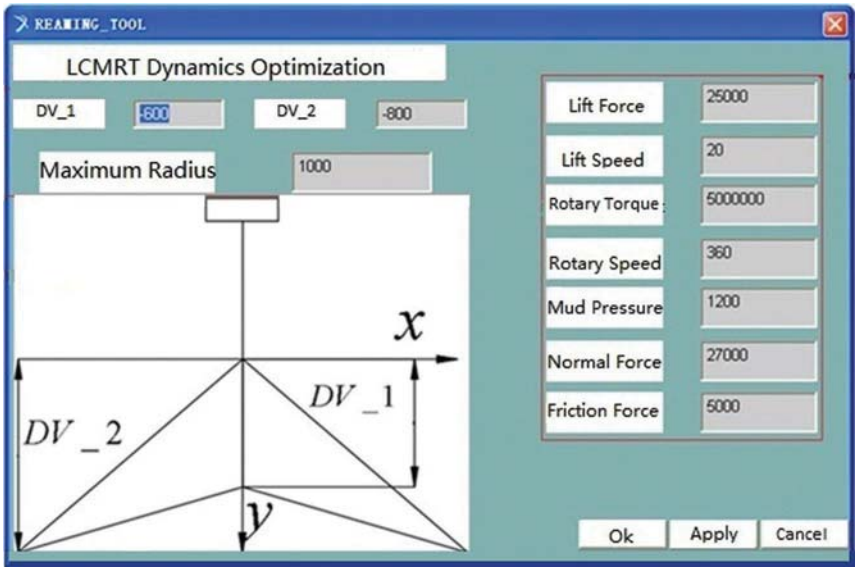

Fig. 16. Graphics user interface (GUI).

4.2. Creation of Optimization Design Variables

Based on the coordinate values of key points which decide the structure of LCMRT, the design variables named as DV_1 and DV_2 are established to characterize the length relation among the cutting bars, connecting rods and mandrel. The effective value range of DV_1 is

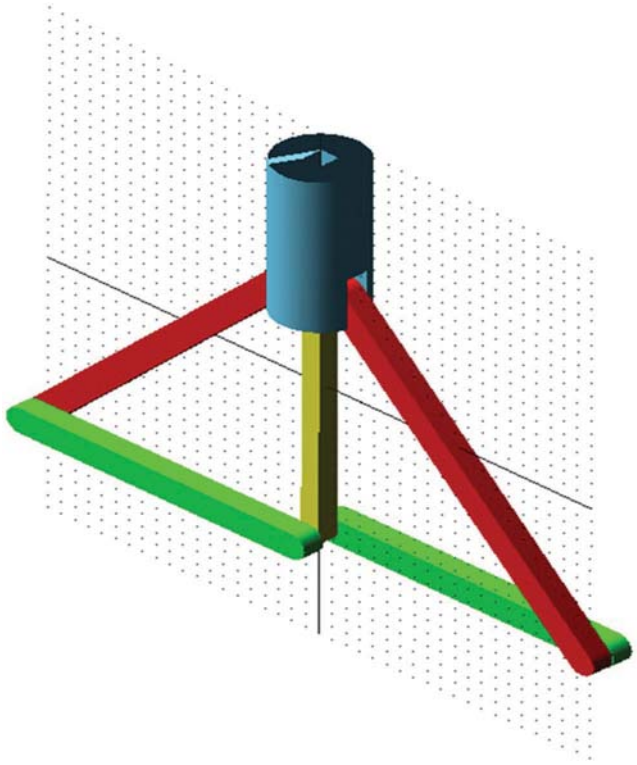

Fig. 17. Parameterized Virtual prototype of LCMRT.

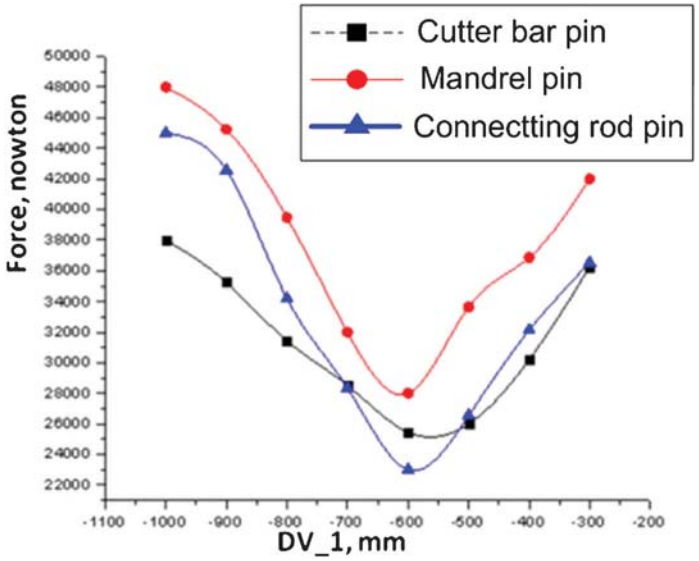

Fig. 18. Stress curves of cutter bar pins, mandrel pins and connecting rod pins when DV_1 is variable.

from −100 to −300, and the normalized value is −600. The effective value range of DV_2 is from −1300 to DV_1, and the normalized value is −600, as described in Figs. 15 and 16.

Meanwhile, the graphics user interface (GUI) is designed to make parameterized modeling more convenient, as shown in Fig. 16. By changing DV_1 and DV_2, the length

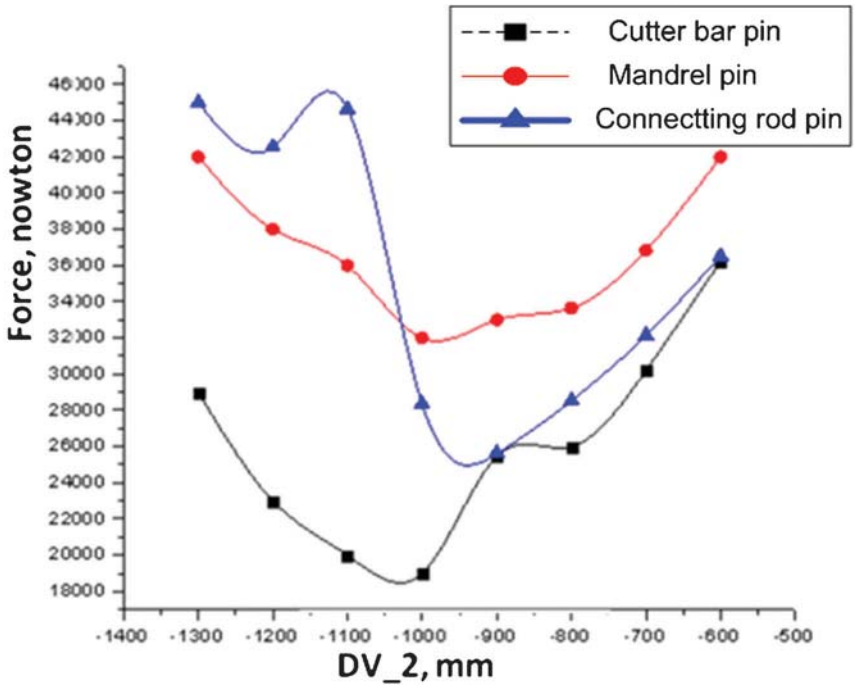

Fig. 19. Stress curves of cutter bar pins, mandrel pins and connecting rod pins when DV_2 is variable.

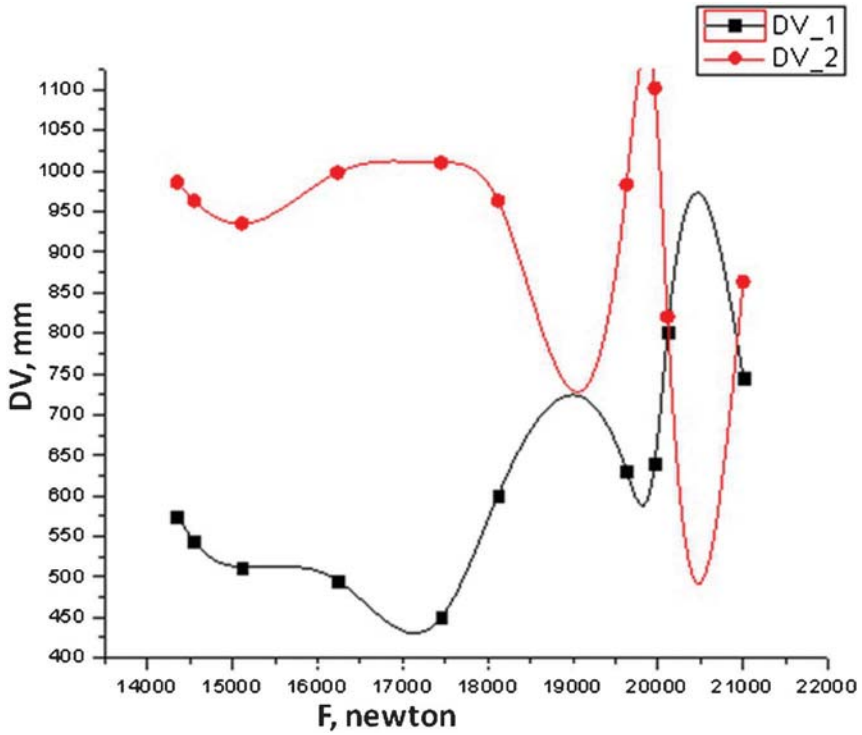

Fig. 20. Curve of DV_1 and DV_2 with the stress of cutter bar pin.

of cutter bars, connecting rods could be modified easily. Moreover, the dynamic simulation and optimization design can be carried out in different structure forms conveniently.

According the detailed size, the geometrical model is built through modeling software. Then, the model established in the modeling software is imported to the ADAMS, and the necessary constraints and forces are acted on the LCMRT. Finally, the virtual prototype of LCMRT is built as shown in Fig. 17.

4.3. Optimization of LCMRT

The concrete relationship between the variables (DV_ 1 and DV_2) and the performance of LCMRT is studied by using ADAMS. Figures 18 and 19 reveal the affection of one variable on pin force when another variable is constant.

1. When DV_2 is −1000 and DV_1 ranges from −1000 to −300, the stress curves of cutting bar pins, mandrel pins and connecting rod pins are shown in Fig. 18.

2. When DV_1 is −600 and DV_2 ranges from −1300 to −600, the stress curves of cutting bar pins, mandrel pins and connecting rod pins are shown in Fig. 19.

Figure 18 shows that when the force acted on cutter bar pins is smallest, the value of DV_1 is −630 mm. Similarly for mandrel pins and connecting rod pins, the value of DV_1 is −590 mm and −520 mm respectively. Figure 19 shows that when the force acted on cutter bar pins is smallest, the value of DV_2 is −1040 mm. Similarly for mandrel pins and connecting rod pins, the value of DV_2 is −980 mm and −950 mm respectively. It is difficult to decide the ultimate parameter value of optimization design.

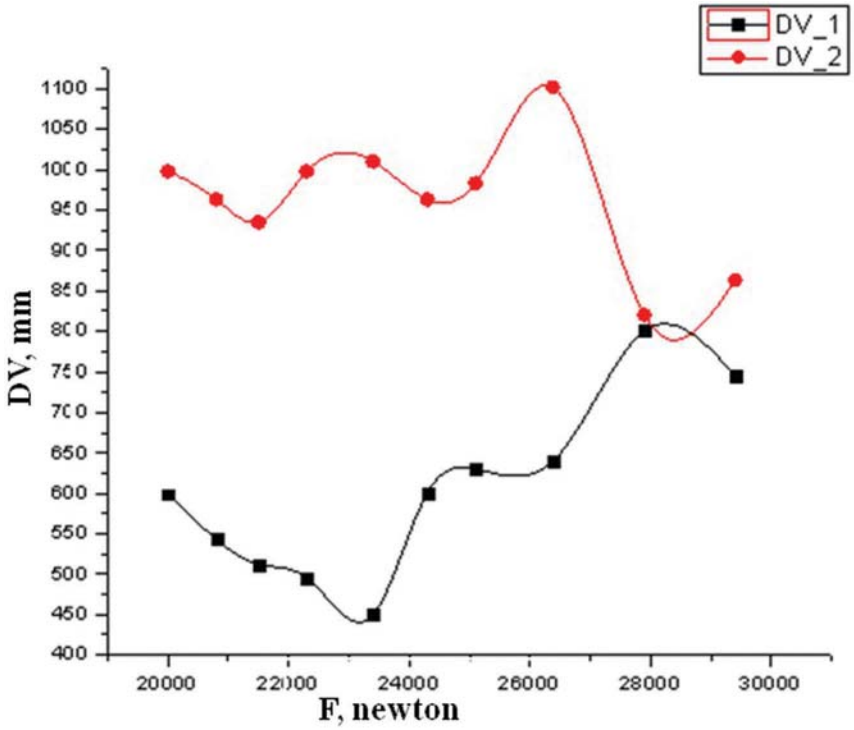

Fig. 21. Curve of DV_1 and DV_2 with the stress of mandrel pin.

According to the results mentioned above, it is noted that the DV_1 and DV_2 are important design variables which affect the performance of LCMRT. Then, the structural optimization analysis is carried out, taking the joint constraint forces as objective function.

Figure 20 shows that the stress of cutter bar pin approaches a minimum value when DV_1 is −575 and DV_2 is −978, so the −575 and −978 is the optimized value of DV_1 and DV_2 respectively for cutter bar joint.

Figure 21 demonstrates that the stress of mandrel pin reaches a minimum value when DV_1 is −600 and DV_2 is −998, then the −600 and −998 is the optimized value of DV_1 and DV_2 respectively for mandrel pin.

Figure 22 depicts that the stress of connecting rod pin achieves a minimum value when DV_1 is −630 and DV_2 is −960. Therefore the −630 and −960 is the optimized value of DV_1 and DV_2 respectively for connecting rod pin.

From the three figures, it is easy to find that connecting rod pins withstand the largest force for all joints, so the force optimization of connecting rod pins should be analyzed first. The values −600 and −1000 are selected as the optimal ones of three group data for DV_1 and DV_2 respectively. The mechanical structure un-optimized is shown in Fig. 23(a) and ones optimized in Fig. 23(b).

4.4. Dynamic Performance of LCMRT Optimized

By building the virtual prototype, carrying out the dynamics simulation and comprehensive analysis, the optimal structure of LCMRT is found. When DV_1 is −600 and DV_2 is −1000, the length of cutter bar and connecting rod is 1670 and 1080 respectively. By using GUI, the structural parameters of LCMRT are easily modified, so

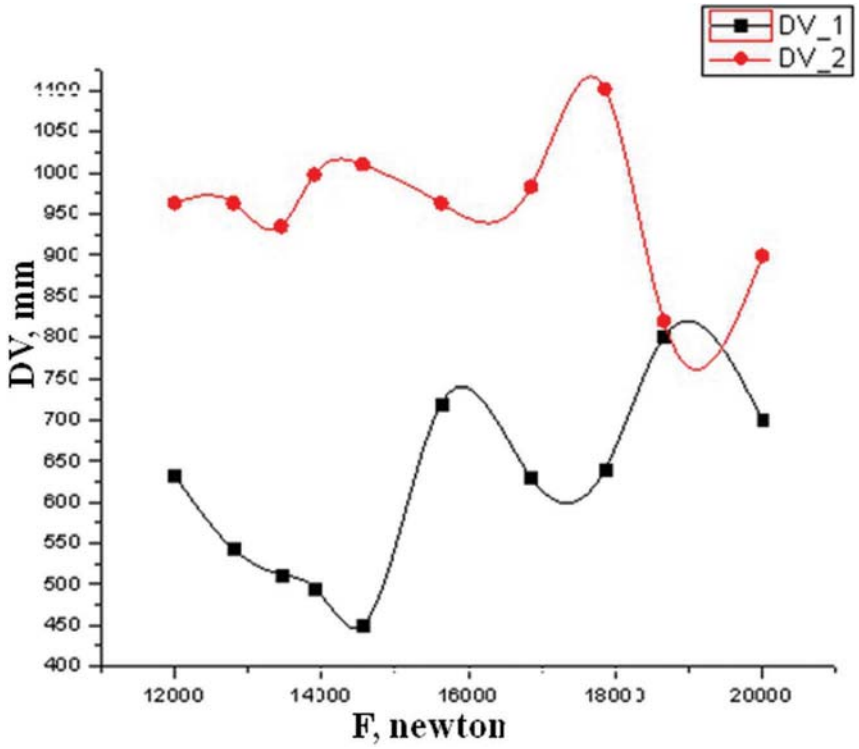

Fig. 22. Curve of DV_1 and DV_2 with the stress of connecting rod pin.

dynamics simulations in different configuration are carried out conveniently. The stress curves are shown in Figs. 24–26.

Comparing Figs. 9–11 with Figs. 24–26, the forces acted on the cutter bar pins, mandrel pins and connecting rod pins are reduced by 10% under normal work condition. Optimized LCMRT

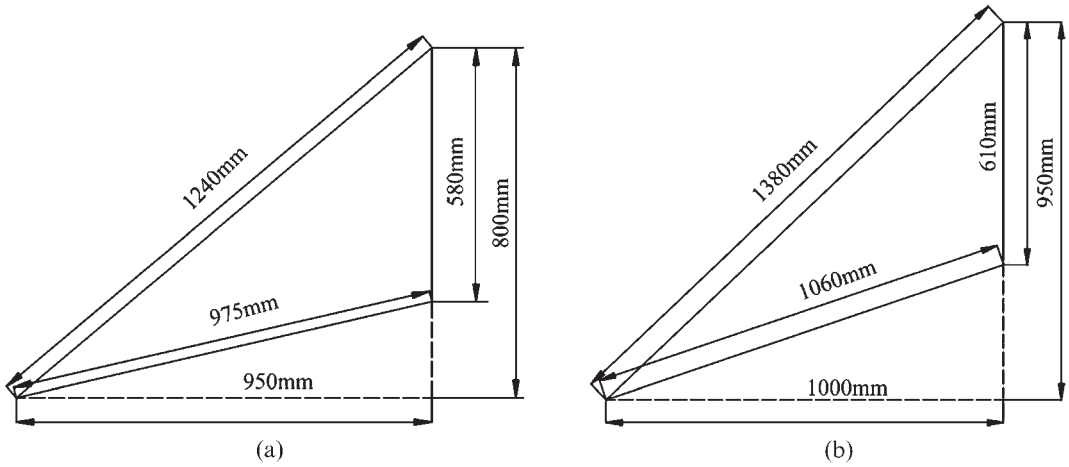

Fig. 23. Mechanical structural size: (a) the un-optimized, (b) the optimized.

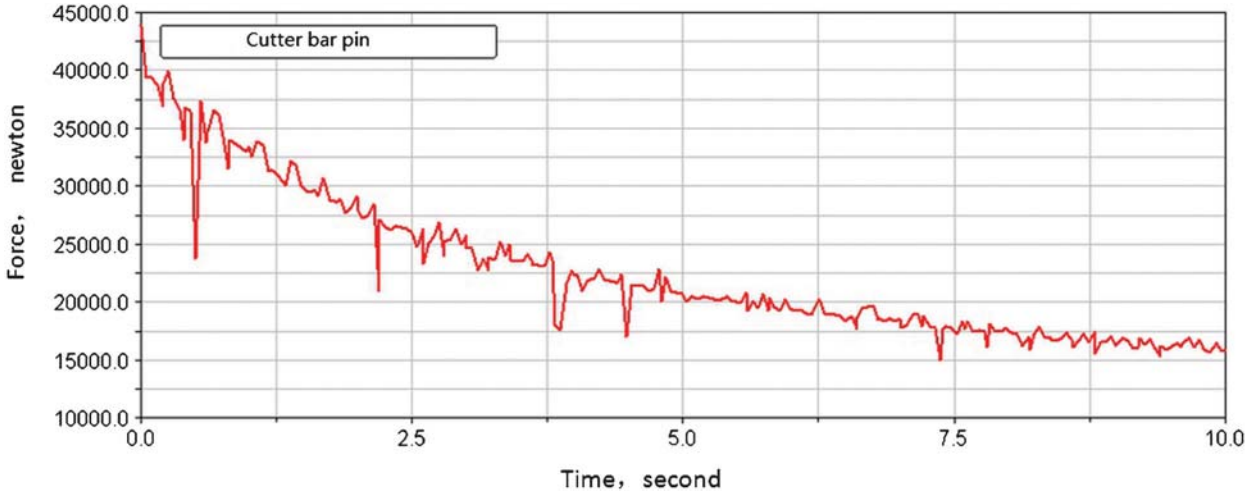

Fig. 24. Stress curve of cutter bar pin.

significantly improve the stress state of each pin. This improvement could reduced the stress of pins and extend the life of LCMRT.

5. CONCLUSION

The conclusion can be summarized as following:

(1) Based on the virtual prototype technique, the software ADAMS is used to carry out the dynamics simulation and parameter optimization design on LCMRT. It can be concluded that virtual prototype technique could reduce the risk of mechanical failure, prolong the mechanical life.

(2) Kinematics and dynamics performance of LCMRT could be acquired conveniently by virtual prototype. This provides a new effective method for the design and analysis of LCMRT.

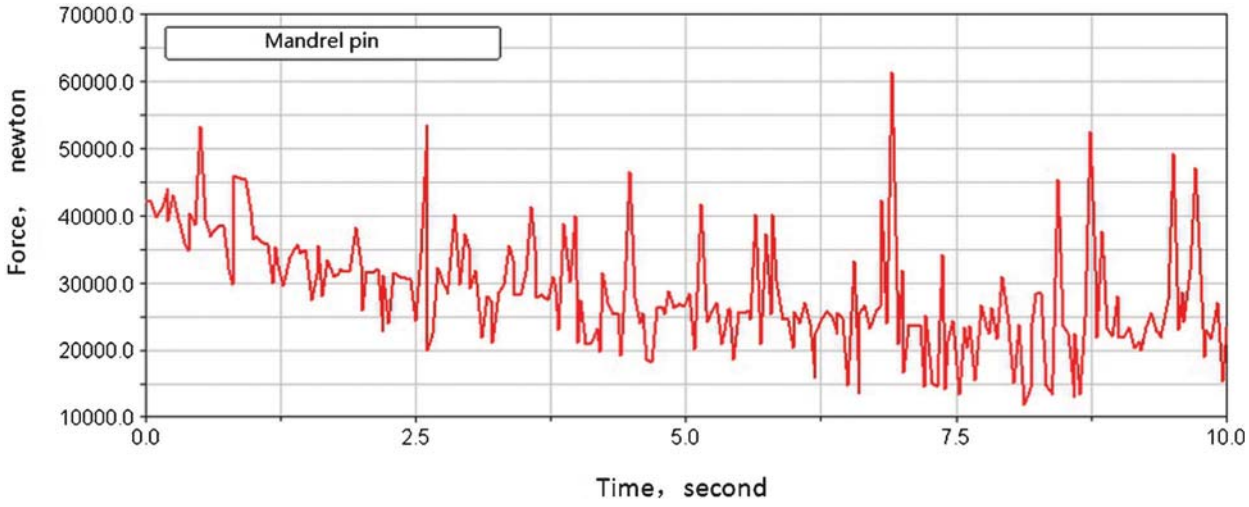

Fig. 25. Stress curve of mandrel pin.

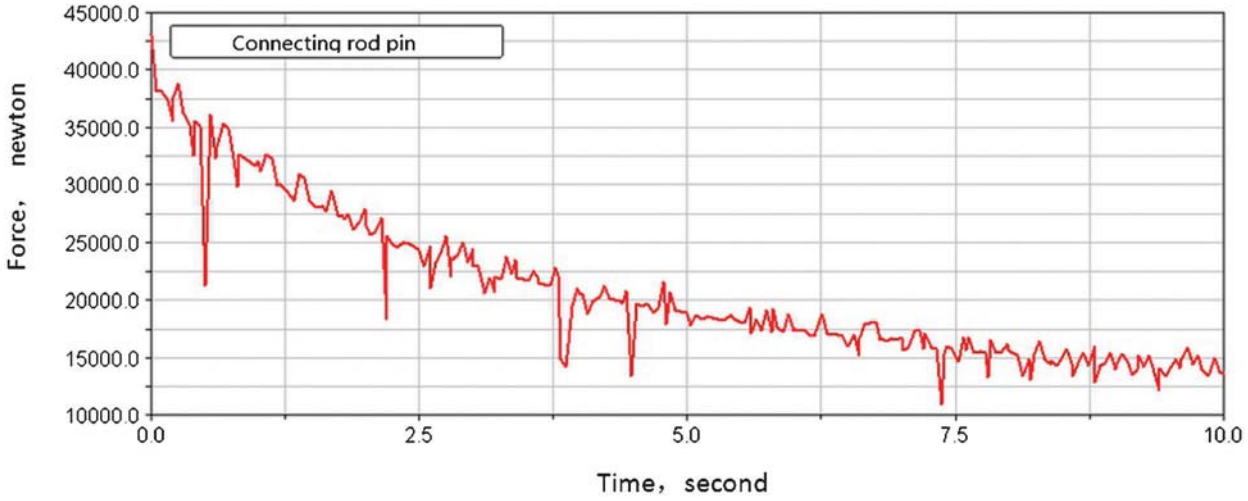

Fig. 26. Stress curve of connecting rod pin.

(4) The performance of LCMRT after optimization is better than that of before optimization. Analysis of the dynamical simulation shows that the minimum force of joints could be the reference for the future research.

(5)The test on the physical prototype which is made according to optimization design shows that the design of LCMRT in new configuration could meet practical requirements under the complex conditions.

The study in this paper could improve the design quality and development efficiency, but also lower the investment of the LCMRT productions.

REFERENCES

1. Wold, M.B., Davidson, S.C., Wu, B., Choi, S.K. and Koenig, R.A., "Cavity completion for coal-bed methane stimulation-an integrated investigation and trial in the Bowen basin, Queensland," *Proceedings of 1995 SPE Annual Technical Conference and Exhibition,* October 22–25, Dallas, Texas, USA, pp. 323–337, 1995.
2. Kull, B., Duff, R.G., Chevron, Alan J., Clarke, Daniel G. Perez and Simon M. Stuart, "Salt drilling while under-reaming behaviors illuminated by distributed down-hole measurements," *Proceedings of 2009 SPE Annual Technical Conference and Exhibition*, New Orleans, Louisiana, USA, pp. 1005–1018, October 4–7, 2009.
3. Shedid, S.A. and Rahman, K., "Experimental investigations of stress-dependent petrophysical properties and reservoir characterization of coalbed methane (CBM)," *Proceedings of Asia Pacific Oil and Gas Conference & Exhibition*, Jakarta, Indonesia, pp. 526–540, August 4–6, 2009.
4. Zhou, J.R., Wang, Y.S., Jing, H.T., Lou, W.X. and Liang, H.M., "Study on techniques for open-hole cavity completed coal-bed gas wells," *Proceedings of the Basic Theoretical Research and Frontier Technology of Drilling Symposium*, Beijing, P.R China, pp. 88–95, October 26–29, 2006.
5. Chakhmakhchev, A., "Worldwide coal-bed methane overview," *Proceedings of the 2007 SPE Hydrocarbon Economics and Evaluation Symposium*, Dallas, Texas, USA, pp. 17–23, April 1–3, 2007.
6. Kalloo, C.L., Attong, D.J. and Steele, H.E., "A novel design bi-center bit successfully drills deep exploration well off the east coast of Trinidad," *Proceedings of the 1994 IADC/ SPE Drilling Conference*, Dallas, Texas, USA, pp. 373–383, February 15–18 1994.

7. Sketchler, B.C., Fielder, C.M. and Lee, B.E., ''New bi-center technology proves effective in slim hole horizontal well,'' *Proceedings of the 1995 SPE/IADC Drilling Conference,* Amsterdam, Netherlands, pp. 559–567, February 28–March 2, 1995.
8. Warren, T.M., Sinor, L.A. and Dykstra, M.W., ''Simultaneous drilling and reaming with fixed blade reamers,'' *Proceedings of the 1995 SPE Annual Technical Conference and Exhibition,* Dallas, Texas, USA, pp. 757–766, October 22–25, 1995.
9. Billman, W.J., Jr. Brown, L.A. and Zaki, M., ''Eccentric tool increases liner size capacity in challenging salt dome application allowing longest horizontal well in Gulf of Sues,'' *Proceedings of the 2000 IADC/SPE Drilling Conference,* New Orleans, Louisiana, USA, pp. 859–869, February 23–25, 2000.
10. Liu, Z.H., ''The coal-bed methane tool with hydraulic machinery,'' *China Petroleum Machinery,* Vol. 36, No. 8, pp. 60–62, 2008.
11. Shabana, Ahmed A., *Dynamics of multi-body systems*, Cambridge University Press, 2005.
12. Feng, Z.Y., Zhang, Y. and Ya, T.L., ''Inverse dynamics of a 2UPS-2RPS parallel mechanism by Newton-Euler formulation,'' *Transactions of the Chinese Society for Agricultural Machinery*, Vol. 40, No. 4, pp. 193–197, 2009.